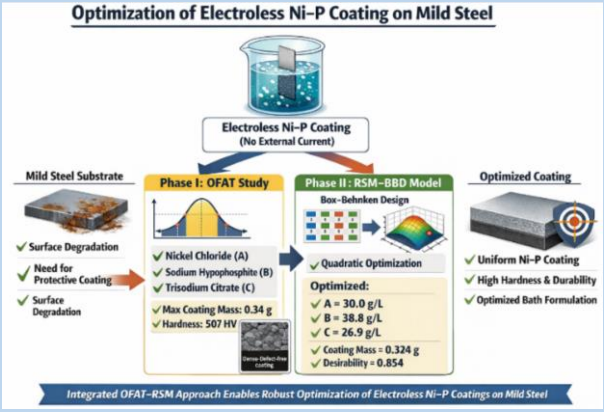
An-Najah University Journal for Research – A
Natural Sciences

Microstructural and Compositional Evaluation of Electroless Nickel-Phosphorus Deposits under Varying Bath Conditions: A Parametric, RSM–BBD and SEM Study

Vijayanand Manickam[1*], Mithun Vinayaka Kulkarni[1], Sivamani Selvaraju[1], Sellappan Narayanagounder[1], Kumaradhas Paulin[1], Rajasekaran Rajangam[2], Said Bakhit Ali Tabook[1], Sharifa Bakhit Ali Al-Awaid[2]
Type: Full Article. Received: 10th Jan. 2026, Accepted: 2nd May 2026, Published: 1st Nov. 2026,
DOI: https://doi.org/10.35552/anujr.a.a2802

Abstract: Mild steel is widely used due to its low cost, ease of fabrication, and versatility, but its susceptibility to surface degradation requires protective coatings to enhance performance and service life. Electroless nickel–phosphorus (ENi–P) coating is preferred as it provides uniform, adherent, and wear-resistant deposits on complex geometries without external electrical current. This study presents a two-phase optimization of an electroless Ni–P bath for mild steel, progressing from single-factor analysis to multivariate modelling. In Phase I, a One-Factor-at-a-Time (OFAT) approach was used to study nickel chloride, sodium hypophosphite, and trisodium citrate individually, each showing a bell-shaped response with an intermediate optimum. The highest coating mass (0.34 g), along with 97.31% Ni, 2.69% P, and 507 HV hardness, was obtained at the central condition (A = 30 g/L, B = 40 g/L, C = 25 g/L). Quadratic fits showed excellent agreement with experimental data, and Solver-based refinement further identified nearby optimal conditions for each parameter. Microstructural analysis confirmed that balanced bath compositions produced compact, defect-free coatings with higher hardness, while deviations led to porosity and reduced performance.



In Phase II, a Box–Behnken Design (RSM) was developed within the Phase I concentration limits to build a second-order predictive model. Response surface analysis confirmed that the optimum lies near the center of the design space and revealed a critical interaction effect: simultaneous increase of sodium hypophosphite and trisodium citrate beyond their optimal levels leads to a sharp reduction in coating mass, reaching a minimum of 0.23 g, which could not be captured through single-factor analysis. The desirability-based optimization identified the optimum at A = 30.0 g/L, B = 38.8 g/L, and C = 26.9 g/L with a predicted coating mass of 0.3240 g (desirability = 0.854). This closely matched the OFAT and Solver results, and the consistent convergence across all methods confirms the robustness of the optimization and highlights.

Keywords: Electroless; Nickel-Phosphorus; Microhardness; OFAT; Parametric Study; Response Surface Methodology; Box–Behnken Design; Interaction Effects; Optimization.

Introduction

The process of Electroless Nickel (ENi) deposition is a widely adopted coating technique used to prepare metallic and composite coatings. It remains highly relevant across various research and industrial fields due to their broad scope of applications. Brenner and Riddell were the first to report about this process [1, 2], in which the reduction of nickel ions was achieved using a strong reducing agent in the absence of externally applied electric current. Since its inception, EN deposition has been regarded as an important method in surface engineering and advanced material synthesis [3].

EN coatings are known to provide many advantages, such as controlled and uniform deposition on components with complex or irregular shapes, excellent resistance to wear [4–6], and corrosion [6, 7], high hardness [8, 9], enhanced electrical conductivity [10], strong solderability and good adhesion. Due to their adaptability and ease of application, EN coatings are widely used in diverse sectors such as renewable energy, automotive, aerospace, biomedical, oil and gas, and electronics.

ENi coatings are generally classified into four types: pure nickel, alloys, poly-alloys, and composites. Alloy and poly-alloy coatings are further divided into binary (e.g., Ni-P, Ni-B), ternary, and quaternary types depending on the number of alloying elements incorporated [11]. Among these Ni-P coatings are particularly important, as phosphorus strongly influences the metallurgical properties of the EN coatings.

Phosphorus content of up to 4 wt.% can enhance hardness and improve wear resistance. Medium-phosphorus coatings (typically 2–4 wt.%) are often tailored to specific applications: 4–7 wt.% phosphorus for decorative finishes, 6–9 wt.% for general industrial use, and 4–10 wt.% for electronic components. High-

1 Mechanical and Chemical Engineering Unit, Department of Engineering and Technology, University of Technology and Applied Sciences, Salalah, Sultanate of Oman.
2 Department of Supportive Requirements, University of Technology and Applied Sciences, Salalah, Sultanate of Oman.
* Corresponding author: vijayanand.manickam@utas.edu.om.
ORCID iD: https://orcid.org/0000-0002-7034-6109

phosphorus coatings (10–14 wt.%) [12] are particularly well suited for exposed to corrosive and acidic environments, such as in oil drilling and coal mining. These coatings can achieve hardness up to 600 Vickers, making them highly durable in harsh service conditions [13]. The electrolyte bath used in EN deposition consists of reducing agents and nickel ions along with supplementary agents such as complex, stabilization and surfactant. Several process parameters including nickel ion concentration, reducing agent concentration, stabilizer type, bath temperature, pH and the plating load play critical role in determining coating quality [14, 15]. Each component plays a specific role in the nickel deposition process [16]. Nickel ions serve as the metal source, the reducing agent supplies the required electrons to convert the metal ions into their metallic form, the complexing agent controls the rate of deposition and helps in prevent the production of excess nickel ions in the bath. [17, 18], stabilizers inhibit bath deposition, and surfactants enhance wettability by lowering solid-liquid interfacial surface tension [18,19].

Numerous studies have explored the influence of deposition parameters on EN coatings. For instance, a uniformly distributed 60 µm-thick NiCr coating was applied to LF2 steel to study parameter effects [20]. Electroless Ni-P plating has been optimised for low-temperature applications by analysing electrolyte composition and plating conditions resulting in stable Ni-P deposits for copper surface finishing in flexible printed circuits [21]. Zou et al. obtained Ni-P coatings with varying phosphorus content (3–11 wt.%) on Cr12MoV die steel by adjusting process parameters. These values were used as inputs to a Back Propagation Neural Network, and the results were further validated through Particle Swarm Optimization [22].

In another study, electroless Ni-P coating with 9.61 wt.% phosphorus was deposited on copper, where RSM and ANOVA analyses revealed that nickel sulphate, and the interaction of sodium hypophosphite with bath temperature, significantly influenced coating microhardness [23, 24]. Efforts to minimize corrosion rate have also involved parametric optimization of Ni–P coatings on copper, with predictive models developed using Artificial Neural Network (ANN) [25]. Xijun et al. reported that optimizing parameters such as ultrasonic power, temperature, and plating speed during electroless nickel plating on AZ91D magnesium alloy significantly improves the coating's hardness, wear resistance, and corrosion resistance [26]. The effect of Lawsonia inermis Linn leaf extract as an additive in alkaline solutions has also been studied, showing that increasing the additive volume from 0.5 mL to 5 mL enhanced Ni–P alloy deposition on mild steel [27]. A PSO-BP neural network was used to study how process parameters influence aluminum content in Ni-P-Al_2O_3 coatings, showing pH and surfactant as the most significant factors with improved coating properties under optimized conditions [28]. Optimization methods such as Simulated Annealing (SA), Genetic Algorithm (GA), and Particle Swarm Optimization (PSO) are widely used beyond engineering applications for solving complex optimization problems [29].

Despite these advances, some challenges remain, particularly concerning coating quality and the uniformity of the deposition parameters. These factors directly influence adhesion strength and compositional control, especially regarding phosphorus and nickel content. Thus, the aim of the proposed research is to produce an electroless nickel-phosphorus (ENi-P) coating on mild steel and to investigate and optimize the procedure systematically. The objective is to refine the critical process parameters to achieve the best outcomes in terms of coating mass and elemental composition, with particular focus on attaining an appropriate balance of nickel and phosphorus in the deposit. To achieve this, a two-phase experimental strategy is adopted. In Phase I, a One-Factor-at-a-Time (OFAT) parametric study is conducted to investigate the individual effect of each bath parameter on coating mass and elemental composition, while maintaining the remaining variables at constant centre values. This approach establishes clear individual-factor response trends and defines the operating ranges for each variable. In Phase II, a Box–Behnken Design (BBD) under Response Surface Methodology (RSM) is applied using the OFAT-derived ranges to construct a second-order polynomial model, quantify interaction effects between factors, and confirm the local optimum through multivariate statistical analysis. This integrated OFAT–RSM approach bridges the clarity of single-variable parametric analysis with the rigour of design-of-experiments (DOE) optimization, providing a comprehensive understanding of the electroless Ni–P deposition process.

Materials and Methods

Specimen preparation with pre-treatment: A mild steel rectangular plate (20 × 25 × 3 mm) was used as the substrate in this study. The plate was first mechanically polished and then disc polished, followed by cleaning with methanol. Surface activation was carried out by acid etching in a 20% H_2SO_4 solution for 2 minutes. Such pre-treatment is essential to achieve a high-quality coating [30, 31].

Electroless Bath: The electroless nickel-phosphorus bath used in this study consisted of analytical grade $NiCl_2$ as the nickel source (30 g/L), $NaPO_2H_2$ as the reducing agent (40 g/L), NH_4Cl as the complexing agent (50 g/L), and $Na_3C_6H_5O_7$ as the stabilizer (25 g/L). The coating process was conducted at 85 ± 5 °C, with the bath temperature continuously monitored and controlled using a proportional-integral-derivative (PID) controller. The pH of the electrolyte was maintained between 8 and 8.5 using an ammonia solution. The electrolyte bath composition and the operating conditions are given in Table 1.

Table (1): Bath composition and the operating conditions.

Nickel Chloride	30 g/L
Sodium hypophosphite	40 g/L
Trisodium citrate	25 g/L
Ammonium chloride	50 g/L
pH	8–8.5
Temperature	85 ± 5 °C
Deposition time	60 minutes

One-factor-at-a-time approach: The One-Factor-at-a-Time (OFAT) approach is an experimental design strategy in which factors are tested individually rather than simultaneously [30]. This method was applied to study both the mass of the deposit and the percentage of nickel and phosphorus in the coating. In the present study, the OFAT approach was employed as a structured parametric study to investigate the individual effect of each bath parameter nickel chloride (A), sodium hypophosphite (B), and trisodium citrate (C) on coating mass and elemental composition, while the remaining two parameters were held constant at their centre values. This approach provides clear, interpretable individual-factor response trends and establishes the operating range for each variable, which were subsequently used as the coded-level boundaries (−1, 0, +1) for the BBD matrix. While the OFAT parametric study cannot capture interaction effects between simultaneously varying factors, it serves as Phase I of the two-phase experimental strategy, directly informing and enabling the multivariate RSM–BBD optimization in Phase II, which are applied in the present study through a Box–Behnken Design (BBD) to provide multivariate statistical validation of the OFAT findings.

Box–Behnken Design for RSM Validation: In Phase II, the same three bath parameters: nickel chloride (A), sodium hypophosphite (B), and trisodium citrate (C) were investigated using a Box–Behnken Design (BBD) under Response Surface Methodology (RSM). The BBD is a three-level, second-order design that estimates linear, quadratic, and two-factor interaction (2FI) effects without requiring a full factorial matrix [32]. The factor levels (−1, 0, +1) were set at the boundaries and midpoint established by the OFAT parametric study (Table 2), ensuring that the RSM design space spans the experimentally validated region. Fifteen runs (Table 6) were conducted, including three centre-point replicates to estimate pure error and test model

adequacy, enabling a rigorous statistical comparison with the OFAT-derived individual-factor trends.

Table (2): Independent factors and their levels.

Bath Components (g/L)	Levels		
	-1	0	+1
A - Nickel Chloride	25	30	35
B - Sodium hypophosphite	30	40	50
C - Trisodium Citrate	20	25	30

Coating process: After surface activation, the sample was immersed in the electroless bath (Fig. 1). During this period, the water bath was allowed sufficient time to reach the required

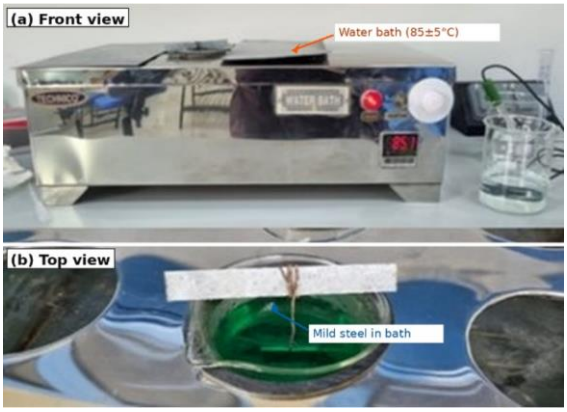


Figure (1): ENi-P coating process on mild steel.

temperature from room temperature, while the pH of the prepared electrolyte was simultaneously adjusted from acidic to alkaline. The ENi-P coating was then carried out for 60 minutes. After plating, the specimens were washed with water and dried.

Weight Measurement: After the coating process the amount of nickel deposited was calculated using the weight gain method. The digital weighing scale was used to weigh the samples before and after the ENi-P coating process. The difference in weight was considered as mass of the deposit on to the mild steel substrate.

Elemental Composition: To obtain accurate quantitative data on the elemental composition of the coatings, the percentages of nickel and phosphorus in the deposits were determined using Positive Material Identification (PMI) equipment at OQBI, Salalah, Sultanate of Oman.

Results and Discussion

Development of ENi-P coatings on mild steel: Ni–P alloy layers were successfully grown on mild steel substrates via the autocatalytic deposition technique. The amount of nickel deposited was calculated using the weight gain method. The details are presented in Table 3.

Table (3): Weight of the samples before and after the ENi-P coating process.

S. No.	Sample ID	Weight before coating (grams)	Weight after coating (grams)
1	S1 - Acidic	14.91	14.97
2	S2 - Alkaline	10.46	10.63

It was observed that samples coated in an electrolyte bath under alkaline conditions exhibited higher nickel deposition than those coated under acidic conditions (Table 3). Consequently, the entire coating process in this study was carried out under alkaline conditions. Additionally, the process parameters were selected based on their significance, as identified through a literature review [33-36].

The selected parameters include the concentrations of nickel ions, the reducing agent, and the stabilizer. The impact of these parameters on various coating properties is examined. In order to study the influence of the concentrations of nickel ions, reducing agent, and stabilizer on the properties of the coatings, the concentrations are varied as presented in Table 2.

Table (4): OFAT parametric study — independent variables and observed responses.

Run No	A	B	C	Output Weight gain (g)	Ni%	P%	Micro Hardness (HV)
1	25	40	25	0.24	93.46	6.54	438
2	30	40	25	0.34	97.31	2.69	507
3	35	40	25	0.31	95.10	4.90	392
4	30	30	25	0.22	91.63	8.37	493
5	30	40	25	0.29	96.99	3.01	512
6	30	50	25	0.21	92.74	7.26	462
7	30	40	20	0.21	95.71	4.29	476
8	30	40	25	0.30	97.15	2.85	493
9	30	40	30	0.28	91.77	8.23	429

A = Nickel chloride (g/L); B = Sodium hypophosphite (g/L); C = Trisodium citrate (g/L). Runs 2, 5, and 8 are replicates at the centre-point condition.

One Factor at a Time (OFAT) Experimentation: In this experimental approach, only one variable is altered at a time, while all other variables are held constant [37, 38, 39]. Using this method, the total number of experiments was fixed at nine as shown in Table 4.

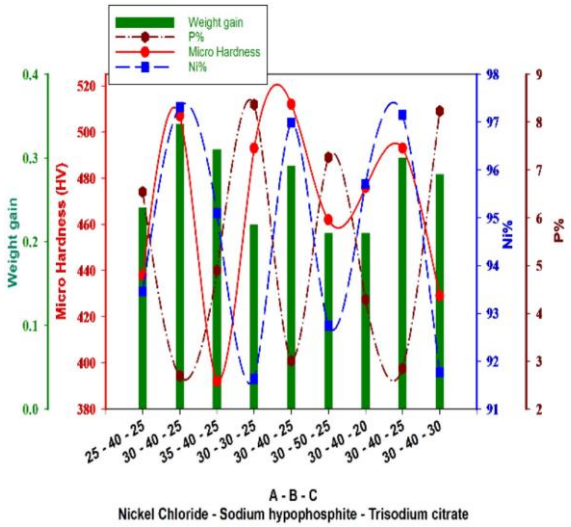


Figure (2): Independent variables vs. dependent parameters.

Accordingly, nine electroless nickel-phosphorus coatings (ENi-P) were carried out. The samples were weighed before and after the coating and the weight gain along with the elemental composition (% of Ni and % of P) was recorded. Based on the experimental results (Fig. 2), the ENi-P coatings were influenced largely by the variations in nickel chloride (A), sodium hypophosphite (B), and trisodium citrate (C) concentrations. In particular, when the nickel chloride was increased by 5 g/L (Runs 1 to 2), the weight gain increased significantly (from 0.24 g to 0.34 g), and the nickel content rose from 93.46 wt.% to 97.31 wt.%. Conversely, the phosphorus content decreased (from 6.54 wt.% to 2.69 wt.%), which was accompanied by an improvement in microhardness (438 HV → 507 HV).

However, a further increase to 35 g/L (Run 3) slightly reduced both coating mass (0.31 g) and microhardness (392 HV). This indicates that an excessive concentration of nickel ions can cause internal stress or uneven deposition, thereby lowering the coating integrity.

The influence of sodium hypophosphite was observed in Runs 4, 5 and 6, where the concentrations was varied at 30, 40, and 50 g/L, respectively, while other factors were unchanged. The highest weight gain, and hardness occurred at 40 g/L (Run 2). At 30 g/L (Run 4), both weight gain and hardness decreased, while phosphorus content increased to 8.37 wt.%, suggesting that the coating became more amorphous and possibly porous. At 50 g/L, the phosphorus content decreased slightly (7.26 wt.%), but the coating thickness (0.21 g) was lower, and the hardness dropped to 462 HV, indicating either inefficient deposition or the formation of brittle phases due to excessive reducing agent.

The effect of trisodium citrate was studied in Runs 7, 8 and 9; corresponding to concentrations of 20, 25 and 30 g/L, respectively, while the values of A and B were held constant. Optimal results were obtained at 25 g/L (Run 2) where the weight gain (0.34 g), nickel content reached 97.31 % and hardness was the highest at 507 HV. Both lower and higher concentrations led to inferior coatings. At 20 g/L (Run 7), early precipitation or uneven plating may have occurred, whereas at 30 g/L (Run 9), over-complexing likely reduced the deposition rate and nickel availability, resulting in lower nickel content and hardness.

The best condition was achieved in Run 2 with A = 30 g/L, B = 40 g/L and C = 25 g/L. This composition produced coatings with maximum nickel, minimum phosphorus, maximum weight gain, and highest microhardness (507 HV). These results demonstrated that a fine balance between the nickel source, reducing agent and stabilizer is critical for achieving dense, uniform and hard electroless Ni-P films on mild steel substrates.

It should be noted that in Table. 4, the runs 2, 5, and 8 represent replicate experiments conducted under identical bath conditions (A = 30 g/L, B = 40 g/L, C = 25 g/L). The results from these replicates yielded a mean weight gain of 0.31 ± 0.03 g, a mean nickel content of 97.15 ± 0.16 wt.%, a mean phosphorus content of 2.85 ± 0.16 wt.%, and a mean microhardness of 504 ± 10 HV, confirming the reproducibility of the coating process under these optimum conditions.

Surface Morphology and Microstructural Evaluation: The input data for Sample 3 were: A = 35 g/L, B = 40 g/L, C = 25 g/L, with responses of 0.31 g weight gain, 95.10% Ni, 4.90% P, and 392 HV microhardness.

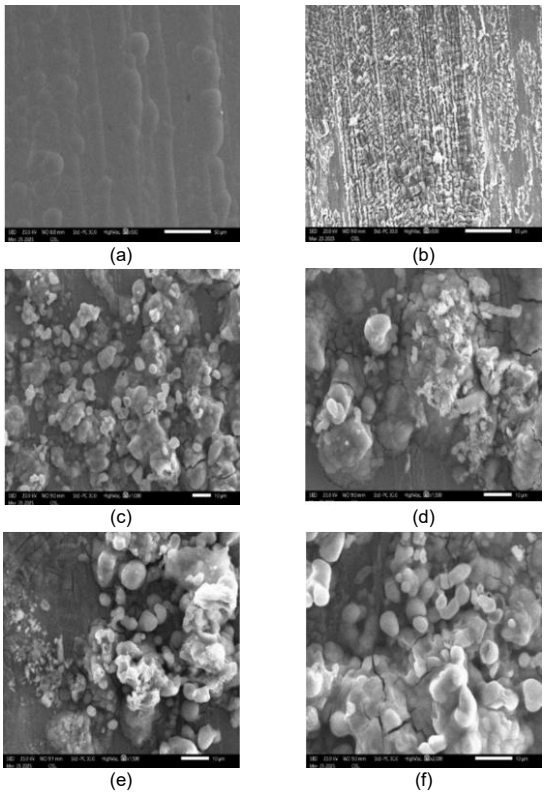


Figure (3): Sample 3 – High nickel concentration effect on morphology.

The SEM image (Fig. 3) reveals a slightly dense nodular structure but a certain level of coarseness and discontinuity. Several micro-cracks and uneven voids are visible, likely due to the high nickel content, which increases internal stress within the coating.

The surface is less than optimally compact, corresponding with reduced microhardness and modest phosphorus content. Without normalizing other parameters, a higher nickel concentration of 35 g/L results in uneven growth and reduced mechanical soundness.

The input data for sample 4 were A = 30 g/L, B = 30 g/L, C = 25 g/L, yielding responses of 0,22 g weight gain, 91.63 wt.% Ni, 8.37 wt.% P and 493 HV. SEM images (Fig. 4) show a relatively smooth granular surface, characteristic of phosphorus rich amorphous Ni-P coating. The grain size appears finer with little visible pores. The higher phosphorus content correlates with increased hardness, although the total coating thickness is comparatively lower.

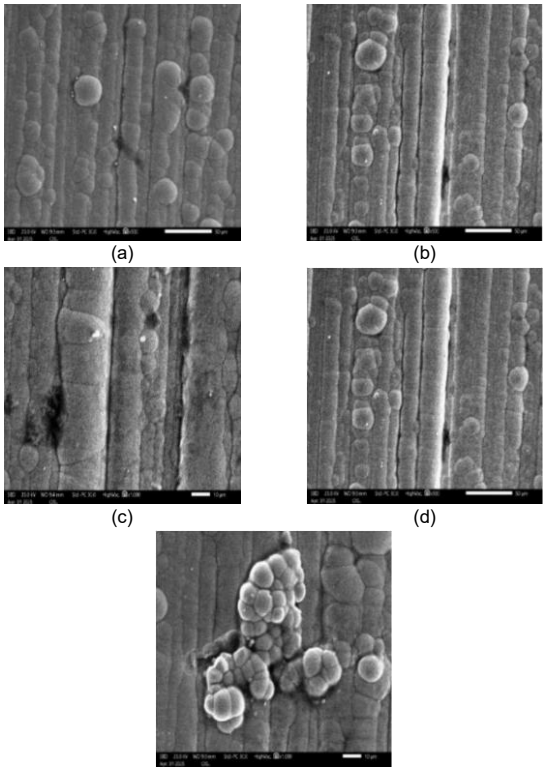


Figure (4): Sample 4 – Influence of low reducing agent on surface texture.

Decreasing concentration of the reducing agent increased phosphorus incorporation but reduced deposition rate and mass.

At the bath composition of A = 30 g/L, B = 40 g/L, and C = 25 g/L, Sample 5 produced a weight gain of 0.29 g, an elemental composition of 96.99 wt.% Ni and 3.01 wt.% P, and a microhardness of 512 HV. As observed in Fig. 5, the SEM micrographs show a uniform, compact nodular microstructure with less microdefects, consistent with the characteristic morphology of low-phosphorus electroless Ni-P deposits.

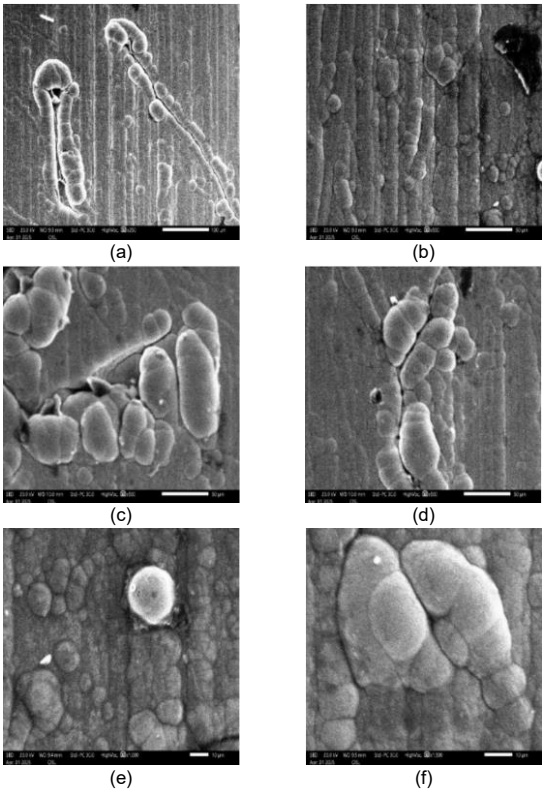


Figure (5): Sample 5 – Optimal coating uniformity and microhardness.

The medium phosphorus level renders the coating microcrystalline and thus increases the hardness. Surface integrity is excellent, with no peeling, or voids observed.

Sample 6 (A = 30 g/L, B = 50 g/L, C = 25 g/L) exhibited responses of and 0.21 g weight gain 92.74 wt.% Ni, 7.26 wt.% P, and 426 HV. SEM images (Fig. 6) reveal a relatively smooth surface having small-sized nodules, but noticeable porosity and irregular cluster formation.

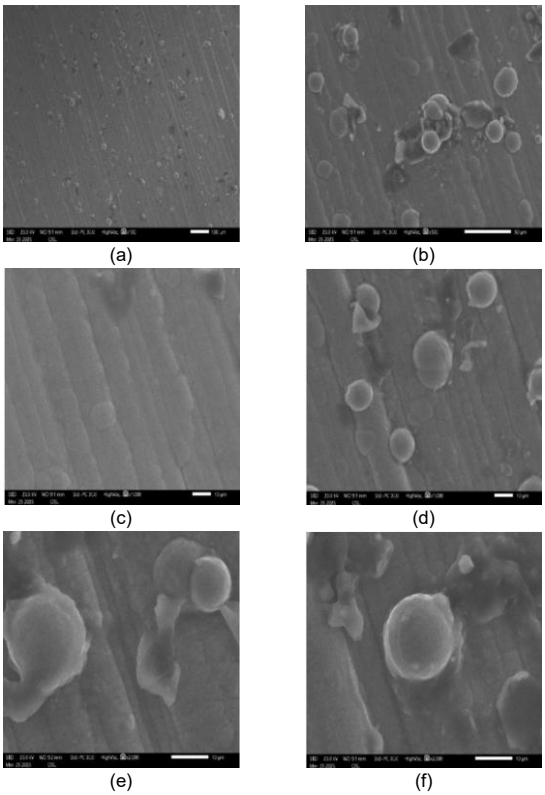


Figure (6): Sample 6 – Impact of excess reducing agent on deposit quality.

The high concentration of reducing agent increased phosphorus content, but the coating compactness and thickness were reduced. Compared to more balanced compositions, the deposit quality was poorer, highlighting the adverse effect of excess hypophosphite.

For Sample 9, the inputs were A = 30 g/L, B = 40 g/L, and C = 30 g/L with responses 0.28 g weight gain, 91.77 wt.% Ni, 8.23 wt.% P and 429 HV. SEM images (Fig. 7) show a loose coating with distinct micro-voids and presence of grain clusters.

High level of stabilizer concentration hindered uniform deposition reducing coating density and continuity. This adversely impacted hardness and the coating quality (reduction in values were observed). Thus, over stabilization has a negative impact on electroless plating, leading to inferior mechanical performance.

SEM analysis was limited to samples representing either optimum coating conditions or distinct morphological deviations. Samples 1 (93.46 wt.% Ni, 6.54 wt.% P, 438 HV) and 7 (95.71 wt.% Ni, 4.29 wt.% P, 476 HV) showed intermediate Ni/P ratios and micro hardness values, consistent with the observed trend of maximum hardness at $_{97\ \text{wt.\% Ni and}}$ 3 wt.% P. Since their properties were intermediate between imaged cases, additional imaging was omitted to avoid redundancy.

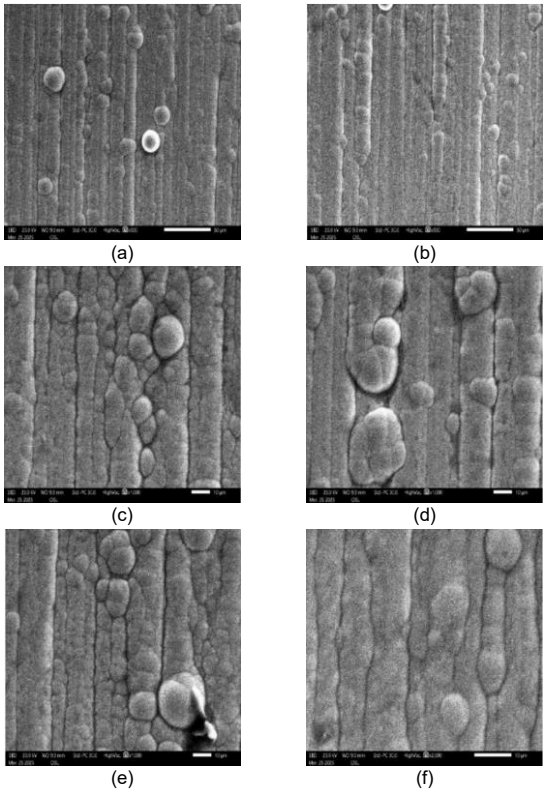


Figure (7): Sample 9 – Effect of high stabilizer content on surface integrity.

Linear Effect of Process Parameters on Mass of the Coating: The individual influence of each bath constituent on deposit mass was examined (Figs. 8–10) through a one-variable-at-a-time approach (Figs. 8–10).

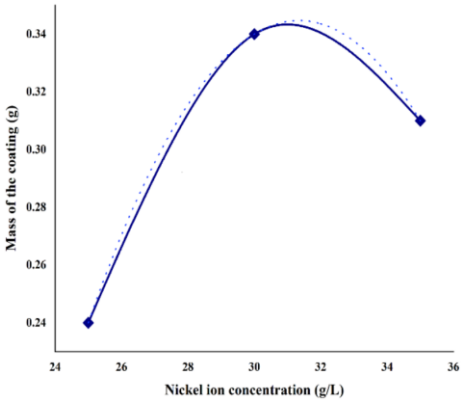


Figure (8): Response trend of various nickel ion concentrations at fixed reducing agent (40 g/L) and complexing agent (25 g/L).

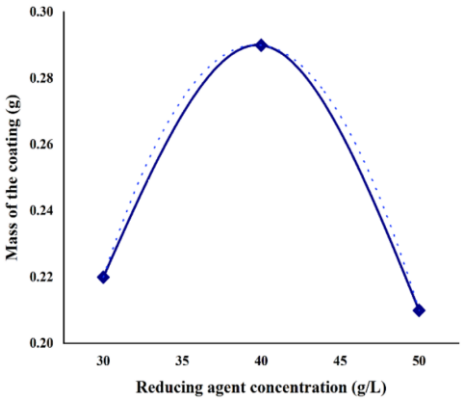


Figure (9): Response trend of various reducing agent concentrations at fixed nickel ion (30 g/L) and stabilizer (25 g/L).

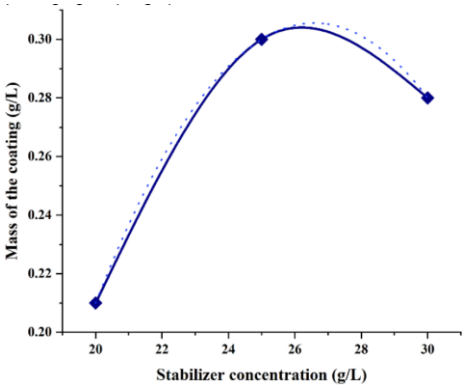


Figure (10): Response trend of various stabilizer concentrations at fixed nickel ion (30 g/L) and reducing agent (40 g/L).

In that a single factor was altered while the remaining variables were held at their central values. Specifically, Fig. 8 illustrates how varying Ni^{2+} levels (25, 30, and 35 g/L) affected deposit mass, with the reducing agent and complexing agent maintained at 40 g/L and 25 g/L, respectively.

Figure 9 illustrates the effect of reducing agent concentration (Sodium hypophosphite) (30, 40 and 50 g/L) with nickel ion and stabilizer concentrations fixed at 30 g/Land reducing agent 40 g/L.

Figure 10 demonstrates the effect of stabilizer concentration (20, 25 and 30 g/L), while maintaining nickel ion at 30 g/L and reducing agent at 40 g/L.

The quadratic regression equations obtained from the OFAT parametric study for nickel chloride (A), sodium hypophosphite (B), and trisodium citrate (C) concentrations are presented as Equations (1), (2), and (3), respectively.

The negative quadratic terms in all three models validate the experimentally observed bell-shaped response of each factor, demonstrating that the coating mass attains a maximum at intermediate concentration levels and subsequently decreases with further increases in each parameter.

$$\text{For } A\text{: } y = -0.0026x^2 + 0.163x - 2.21 \quad (1)$$

$$\text{For } B\text{: } y = -0.0007x^2 + 0.0595x - 0.89 \quad (2)$$

$$\text{For } C\text{: } y = -0.0022x^2 + 0.117x - 1.25 \quad (3)$$

The maximum nickel deposition of 0.34 g was achieved at the optimal concentrations of 30 g/L nickel ion, 40 g/L reducing agent, and 25 g/L stabilizer. As shown in Figs 8–10, reducing the concentration of the reducing agent leads to a decrease in phosphorus content. Similarly, increasing the nickel ion and stabilizer concentrations in the solution reduces the phosphorus content in the coating.

These findings highlight the critical role of the concentration ratio between nickel ions, reducing agent, and stabilizer. Asier Salicio-Paz et.al [35] also reported a comparable trend.

Elemental Composition of Coating: Figure 11 illustrates the variation in coating composition with nickel ion concentration, while keeping the reducing agent at 40 g/L and the stabilizer at 25 g/L. The highest nickel content (97.31wt.%), with a corresponding phosphorus content of 2.69%, is observed at 30 g/L. The results indicate that increasing nickel ion concentration initially enhances deposition, but beyond this level, further addition leads to a decline, likely due to the fixed amounts of reducing agent and stabilizer.

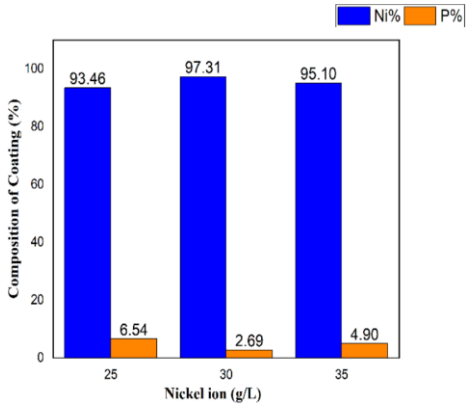


Figure (11): Elemental composition of the coating on the concentrations of nickel ion, at constant concentration of reducing agent 40 g/L and stabiliser 25 g/L.

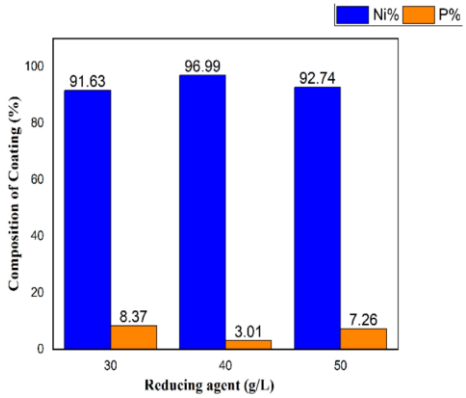


Figure (12): Elemental composition of the coating on the concentrations of reducing agent, at constant concentration of nickel ion 30 g/L and stabiliser 25 g/L.

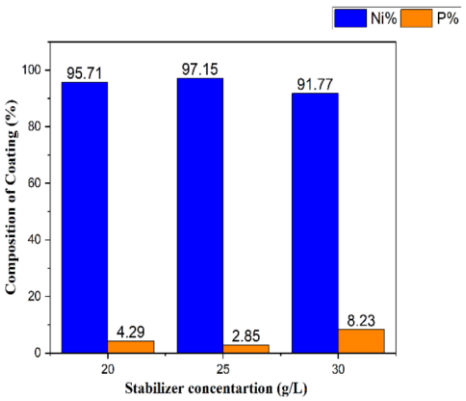


Figure (13): Elemental composition of the coating on the concentrations of stabilizer, at constant concentration of nickel ion 30 g/L and reducing agent 40 g/L.

The highest nickel content (96.99 wt.%) was obtained at 40 g/L reducing agent, with at 3.01 wt.% of P.

Figure 13 depicts the effect of stabilizer concentration (20, 25, and 30 g/L) while maintaining nickel ion and reducing agent at 30 g/L and 40 g/L, respectively. At 25 g/L stabilizer, the coating achieved 97.15 wt.% nickel and 2.58 wt.% phosphorus. Figures 11–13 presents the variation of nickel and phosphorus content with different bath compositions.

Figure 12 illustrates that higher reducing agent concentrations increase phosphorus content, while Figure 13 reveals a similar effect with stabilizer concentration. These results align with the electroless deposition mechanism and are consistent with findings reported by Choudhury et al. [40]

Regression Equation: A key application of the regression equation is to allow estimation of the value of the dependent variable (Y) with known values of the independent variables (X) [40]. In this study, regression models were developed to describe the effect of nickel ion concentration (A), reducing agent concentration (B), and stabilizer concentration (C) on the coating mass. The equations (1-3) were generated using Microsoft Excel and serve as analytical tools to predict coating performance and identify optimum processing conditions.

Solver, an optimization tool available in Microsoft Excel, was employed to determine the optimal values of the process parameters under predefined constraints.

The objective function was set to maximize the coating mass, while the concentration ranges were restricted according to the experimental design.

The Solver results (Fig. 14, Table 5) confirm that the optimal concentrations of nickel ion, reducing agent, and stabilizer are 31.5 g/L, 42.5 g/L, and 26.7 g/L, respectively. These conditions correspond to the maximum achievable coating mass within the imposed experimental limits, thereby validating the regression models as effective predictive tools.

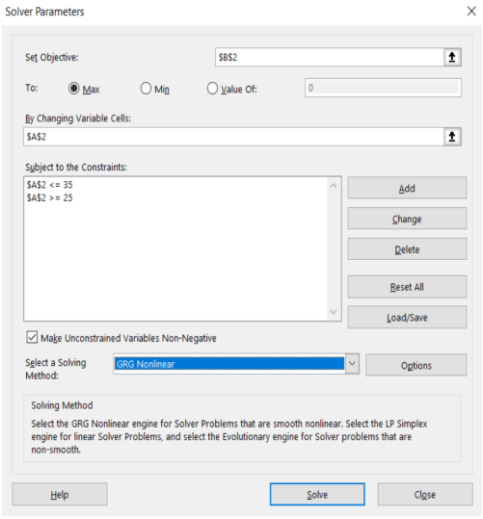


Figure (14): Solver parameters to identify the optimal concentration of source of nickel ions.

Confirmatory experimental runs were conducted at the concentrations predicted to be optimal by the Solver.

The resulting coating mass and elemental composition exhibited trends consistent with the Solver's predictions, thereby validating the underlying regression model.

This consistency underscores the effectiveness of combining Solver-based optimization with experimental verification to ensure the practical relevance of the optimized parameters.

Table (5): Input parameters for the solver.

Variable (X)	Objective function	Constraints	Optimum value in grams	
			X	Y (Output)
A	Maximization	≥ 25 and ≤ 35	31.5	0.35
B		≥ 30 and ≤ 50	42.5	0.38
C		≥ 20 and ≤ 30	26.7	0.31

A = Nickel chloride; B = Sodium hypophosphite; C = Trisodium citrate. All concentrations in g/L.

RSM–Box–Behnken Design: Experimental Runs and Statistical Validation: Fifteen experimental runs were performed according to the BBD matrix (Table 6). The centre-point combination (A = 30 g/L, B = 40 g/L, C = 25 g/L) was replicated in Runs 1, 8, and 11, yielding weight gains of 0.34, 0.32, and 0.31 g respectively (mean: 0.323 ± 0.015 g). This close agreement confirms the reproducibility of the deposition process.

Table (6): Box–Behnken Design experimental runs and observed coating weight gain.

Run No	A	B	C	Output Weight Gain (g)
1	30	40	25	0.34
2	25	40	30	0.26
3	35	50	25	0.24
4	25	30	25	0.27
5	35	30	25	0.27
6	30	30	20	0.25
7	35	40	20	0.26
8	30	40	25	0.32
9	25	40	20	0.26
10	30	50	30	0.23
11	30	40	25	0.31
12	35	40	30	0.26
13	30	50	20	0.25
14	30	30	30	0.25
15	25	50	25	0.24

A = Nickel chloride (g/L); B = Sodium hypophosphite (g/L); C = Trisodium citrate (g/L). Runs 1, 8, and 11 are replicates at the centre-point condition.

Parametric Study to Multivariate Optimization: OFAT–RSM Integration: The OFAT parametric study (Phase I) investigated the individual effect of each bath parameter and identified the optimum at A = 30 g/L, B = 40 g/L, and C = 25 g/L, yielding a maximum coating mass of 0.34 g. Because OFAT

varies one factor at a time while holding all others constant, it cannot detect interaction effects between simultaneously varying parameters. These OFAT-derived ranges were therefore used to define the three coded levels (−1, 0, +1) for the BBD matrix, and the RSM–BBD analysis (Phase II) was applied to quantify interaction effects and provide multivariate statistical validation [41]. The transition from OFAT to RSM–BBD thus represents a logical and complementary progression, not a repetition of experiments.

Table (7): ANOVA for the RSM–BBD quadratic model of Ni–P coating weight gain.

Source	Sum of Squares	df	Mean Square	F-value	p-value	
Model	0.0132	9	0.0015	10.21	0.0099	significant
A-Nickel Chloride	0.0000	1	0.0000	0.0000	1.0000	
B-Sodium hypophosphite	0.0008	1	0.0008	5.58	0.0646	
C-Trisodium citrate	0.0000	1	0.0000	0.3488	0.5805	
AB	0.0000	1	0.0000	0.0000	1.0000	
AC	0.0000	1	0.0000	0.0000	1.0000	
BC	0.0001	1	0.0001	0.6977	0.4416	
A^2	0.0026	1	0.0026	18.32	0.0079	
B^2	0.0064	1	0.0064	44.72	0.0011	
C^2	0.0050	1	0.0050	34.63	0.0020	
Residual	0.0007	5	0.0001			
Lack of Fit	0.0003	3	0.0001	0.3571	0.7940	not significant
Pure Error	0.0005	2	0.0002			
Cor Total	0.0139	14				

The ANOVA results (Table 7) indicate that the RSM–BBD quadratic model is statistically significant (F = 10.21, p = 0.0099), showing that it effectively represents the relationship between bath parameters and coating weight gain. A p-value of less than 0.05 ($p < 0.05$) was considered statistically significant [41, 42]. The non-significant lack of fit (p = 0.7940) confirms that the predicted values closely match the experimental results, indicating good model accuracy. Among the linear terms, sodium hypophosphite shows a noticeable effect, while nickel chloride and trisodium citrate appear insignificant due to their symmetric, bell-shaped behaviour around the optimum, Whereas, on one side of the optimum, the coating weight increases, beyond the optimum, it decreases; as a result, their actual influence is captured through the quadratic terms. All quadratic terms are highly significant, highlighting the strong curvature of the response and supporting the bell-shaped trends observed in the OFAT study, with sodium hypophosphite being the most sensitive parameter. The interaction terms are not statistically significant, likely due to the dominance of quadratic effects, the narrow experimental range, and design limitations, suggesting that the parameters largely act independently within the studied region, which simplifies optimization. However, the response surface and contour plots derived from the significant model still provide useful qualitative insights into combined parameter behaviour and support the ANOVA findings.

Fit Statistics: The model summary (Table 8) shows that the adjusted R^2 and predicted R^2 differ by less than 0.2, confirming a good model fit with no overfitting. The adequate precision ratio exceeds 4, validating the model for navigating the design space.

Table (8): Model summary statistics for RSM–BBD response.

Source	Sequential p-value	Lack of Fit p-value	A-R^2	P-R^2	
Linear	0.8674	0.1512	-0.1949	-0.3043	
2FI	0.9957	0.1043	-0.6303	-0.9922	
Quadratic	**0.0014**	**0.7940**	**0.8556**	**0.6365**	**Suggested**
Cubic	0.7940		0.7649		Aliased

2FI = Two-factor interaction model; A-R^2 = Adjusted R^2; P-R^2 = Predicted R^2.

The second-order polynomial regression equation (Figure 15) shows positive linear coefficients for A and B at centre-point levels and negative quadratic coefficients for all three factors, consistent with the bell-shaped OFAT responses in Figures 8–10.

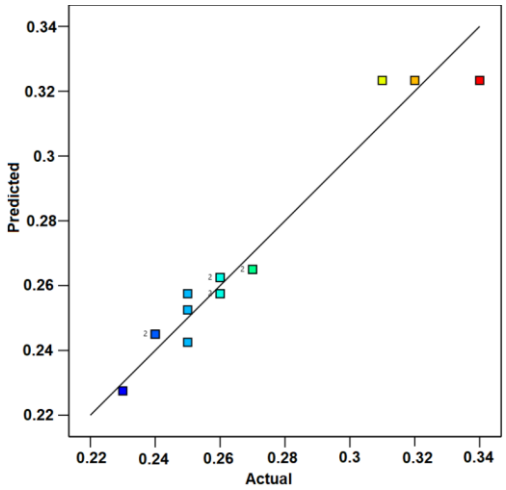


Figure (15): Regression model coefficients for the RSM–BBD second-order polynomial equation.

Actual vs. Predicted Values: compares experimental weight gain with RSM-predicted values for all 15 runs. The mean absolute error is approximately 0.006 g (less than 2.5% of the maximum observed value), validating the model as a reliable predictive tool. The coded regression equation validates the RSM model for maximizing coating weight gain, with negative quadratic coefficients indicating a concave downward response surface and confirming a true maximum within the experimental design space [40, 41]. **The coded factor equation obtained from BBD is given in Equation (4):**

$$\text{Weight Gain} = +0.3233 + 0.0000A - 0.0100B - 0.0025C + 0.0000AB + 0.0000AC - 0.0050BC - 0.0267A^2 - 0.0417B^2 - 0.0367C^2 \quad (4)$$

Interaction Effects: The 3D response surface plots (Figures 16–18) quantify the simultaneous influence of paired bath parameters on coating weight gain — information that is structurally inaccessible to the OFAT approach, which varies only one factor at a time while holding all others fixed. Each surface plot is discussed below with explicit reference to the corresponding OFAT trend to highlight where the two methods agree and where interaction effects introduce behaviour that single-variable experiments would miss or misrepresent.

Figure 16 presents the 3D response surface plot showing the interaction effect of nickel chloride (A) and sodium hypophosphite (B) on coating weight gain, with trisodium citrate fixed at 25 g/L.

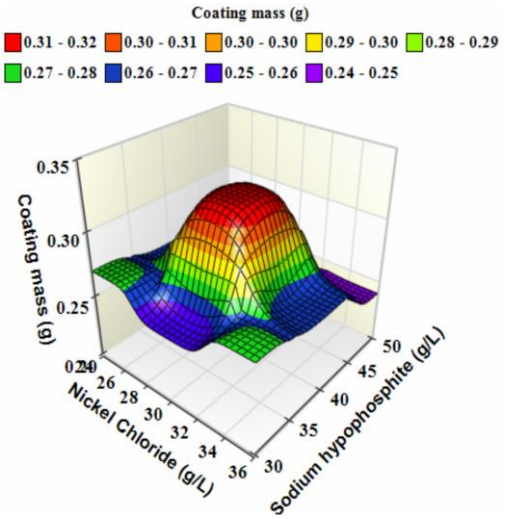


Figure (16): 3D response surface: interaction between nickel chloride (A) and sodium hypophosphite (B) on weight gain (trisodium citrate fixed at 25 g/L).

The surface exhibits a smooth dome-shaped curvature with a distinct peak, indicating that maximum coating mass is achieved at intermediate levels of both parameters. The peak weight gain of 0.34 g is observed at approximately A = 30 g/L and B = 40 g/L. Moving away from these optimal values in either direction by increasing or decreasing either parameter results in a progressive decline in coating mass.

From the topmost point of the dome, a steeper slope along the X-axis compared to the Z-axis confirms that sodium hypophosphite concentration has a stronger influence on coating weight gain than nickel chloride within the studied range, which is consistent with the ANOVA result where B^2 recorded the highest F-value of 44.72.

Figure 17 presents the 3D response surface for the combined effect of nickel chloride (A) and trisodium citrate (C) on coating mass at a fixed sodium hypophosphite level of 40 g/L.

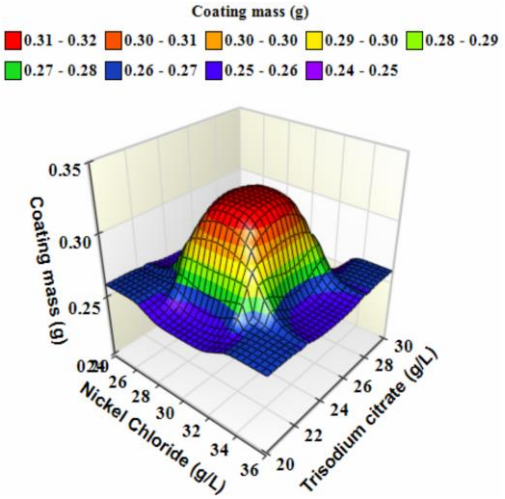


Figure (17): 3D response surface: interaction between nickel chloride (A) and trisodium citrate (C) on weight gain (sodium hypophosphite fixed at 40 g/L).

A clear dome-shaped surface indicates a well-defined maximum within the experimental range, with the highest coating mass (0.31–0.32 g) occurring at A = 30 g/L and C = 25 g/L. Deviating from these optimal values in any direction leads to a gradual decline in coating mass. The drop is more pronounced at higher trisodium citrate levels due to over-complexing, which limits nickel ion availability, while lower concentrations result in poor bath stability. A similar bell-shaped trend is observed for nickel chloride, where both low and high concentrations reduce deposition efficiency.

Figure 18 shows the 3D response surface for the combined effect of sodium hypophosphite (B) and trisodium citrate (C) on coating mass at a fixed nickel chloride level of 30 g/L.

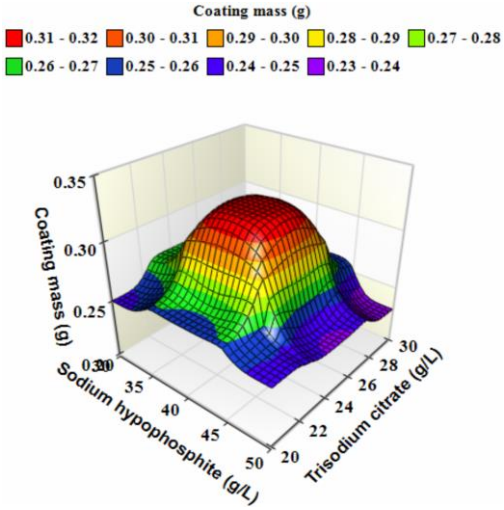


Figure (18): 3D response surface: interaction between sodium hypophosphite (B) and trisodium citrate (C) on weight gain (nickel chloride fixed at 30 g/L).

A clear dome-shaped surface indicates a well-defined maximum, with the highest coating mass (0.31–0.32 g) occurring at B = 40 g/L and C = 25 g/L, while values decrease progressively as either parameter moves away from this optimum. The surface is steepest along the B component axis, confirming sodium hypophosphite as the most sensitive parameter, where even small deviations significantly reduce coating mass. Lower B levels limit the reduction of nickel ions, while higher levels promote excess phosphorus deposition, both leading to reduced performance. The lowest coating mass (0.23–0.24 g) is observed when both B and C are at their highest levels, highlighting the negative combined effect at extreme concentrations.

RSM Optimization: Following the OFAT study, the optimal bath composition was further refined using two independent optimization methods to validate the results. First, MS Excel Solver was applied to the individual quadratic equations, optimizing each parameter within its experimental range and predicting optima at A = 31.5 g/L, B = 42.5 g/L, and C = 26.7 g/L. Second, Design Expert software used a desirability-based approach on the RSM–BBD model to simultaneously optimize all parameters, yielding an optimum at A = 30.0 g/L, B = 38.8 g/L, and C = 26.9 g/L with a desirability of 0.854 (Figure 19). Both methods converge to a similar optimal region, indicating strong agreement despite their different approaches.

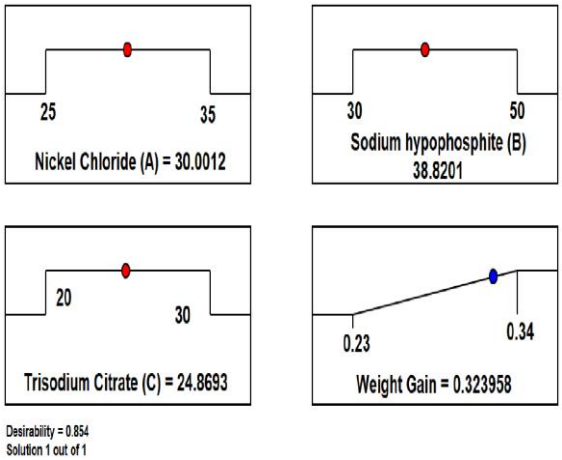


Figure (19): RSM optimization plot: desirability function and predicted optimal concentrations for maximum Ni–P coating weight gain.

This consistency confirms that the true optimum lies within a narrow concentration range and closely matches the

experimental maximum coating mass of 0.34 g observed in the OFAT study, demonstrating the reliability of the overall optimization strategy.

Conclusion

Electroless nickel-phosphorus (Ni–P) coatings were successfully deposited on mild steel substrates, and the effects of nickel chloride (A), sodium hypophosphite (B), and trisodium citrate (C) on coating mass and elemental composition were systematically investigated using a two-phase OFAT–RSM experimental strategy.

In Phase I, the OFAT parametric study established that all three parameters exhibit bell-shaped individual responses, with the optimum coating mass of 0.34 g achieved at A = 30 g/L, B = 40 g/L, and C = 25 g/L, corresponding to 97.31% Ni, 2.69% P, and a microhardness of 507 HV. Individual quadratic regression equations fitted the experimental data with $R^2 = 1$, and MS Excel Solver refined the optimal concentrations to A = 31.5 g/L, B = 42.5 g/L, and C = 26.7 g/L. SEM characterization confirmed that optimal bath compositions produced dense, uniform coatings with minimal porosity, while excess or deficient parameter levels resulted in coarser morphologies and reduced hardness.

In Phase II, the RSM–BBD quadratic model was statistically significant ($F = 10.21$, $p = 0.0099$) with a non-significant Lack of Fit ($p = 0.7940$), validating the model reliability. All three quadratic terms were highly significant ($p < 0.01$), statistically confirming the bell-shaped responses observed in Phase I. The two-factor interaction terms were not significant, indicating that the parameters act predominantly independently within the studied ranges, simplifying process control. The 3D response surface plots provided clear visual confirmation of the optimum, with the B×C surface identifying the most practically important finding: simultaneous excess of sodium hypophosphite and trisodium citrate produces the lowest coating mass of 0.23 g, a compounded effect invisible to single-variable analysis.

Design Expert numerical optimization predicted A = 30.0 g/L, B = 38.8 g/L, and C = 26.9 g/L with a predicted coating mass of 0.3240 g and desirability of 0.854, closely agreeing with both the OFAT optimum and Solver predictions. The three-way convergence of all optimization approaches confirms the reliability of the findings and validates the two-phase OFAT–RSM strategy as an effective approach for comprehensive optimization of electroless Ni–P bath compositions on mild steel.

Disclosure Statement

- **Ethics approval and consent to participate:** Not applicable.
- **Consent for publication:** The authors permit the Publisher to publish the Work.
- **Availability of data and materials:** The raw data required to reproduce these findings are available in the body and illustrations of this manuscript.
- **Author's contribution:** The authors confirm contribution to the paper as follows: VM: Conceptualization, Methodology, Experimentation, Analysis and Draft & Final manuscript preparation. MVK: Literature review, Critical review and Final manuscript preparation. SS: Methodology. SN: Supervision. KP: Methodology. RR: Methodology and Experimentation. SBT: Experimentation. SBA: Experimentation. All authors reviewed the results and approved the final version of the manuscript.
- **Funding:** The authors gratefully acknowledge the University of Technology and Applied Sciences – Salalah for supporting this study through the Internal Research Funding Project, titled: “Development of Electroless Nickel (ENi-P/B) Coatings on Mild Steel for Property Enhancement”.
- **Conflicts of interest:** The authors declare that there is no conflict of interest regarding the publication of this article.
- **Acknowledgements:** The authors are grateful to Mr. Ali Al Zawamri, Team Lead, Asset Integrity – OQBi, Salalah, for granting access to the equipment used in the elemental composition analysis.

Open Access

This article is licensed under a Creative Commons Attribution 4.0 International License, which permits use, sharing, adaptation, distribution and reproduction in any medium or format, as long as you give appropriate credit to the original author(s) and the source, provide a link to the Creative Commons licence, and indicate if changes were made. The images or other third party material in this article are included in the article's Creative Commons licence, unless indicated otherwise in a credit line to the material. If material is not included in the article's Creative Commons licence and your intended use is not permitted by statutory regulation or exceeds the permitted use, you will need to obtain permission directly from the copyright holder. To view a copy of this license, visit https://creativecommons.org/licenses/by-nc/4.0/

References

1] Selvan RA, Thakur DG, Seeman M, Muraliraja R, Ansari MI. Modelling and optimisation of ENi-P-TiO2 coatings synthesised with Zwitterionic surfactant on naval grade AH36 Steel. InSadhana Acad. Proc. Eng. Sci. 2022 Jun 15. https://doi.org/10.1007/s12046-022-01890-7

2] Wang C, Zhai H, Lewis D, Gong H, Liu X, Fernando A. Solvent-driven electroless nickel coatings on polymers: interface engineering, microstructure, and applications. Coatings. 2025 Aug 1;15(8):898. https://doi.org/10.3390/coatings15080898

3] Ghosh S, Bose B, Dolui C, Karmakar P, Pal B, Kumar A, Hoque SK. Tribological Performance Analysis of Electroless Nickel Coated Mild Steel: A Comparative Experimental Study. InE3S Web of Conferences 2023 (Vol. 405, p. 04040). EDP Sciences. https://doi.org/10.1051/e3sconf/202340504040

4] Ahmad M, Samra AS, Habib S, Kahraman R, Mansoor B, Shakoor RA. Mechanical properties and corrosion resistance of electroless deposited Ni-P-Y2O3 nanocomposite coatings for industrial applications. Scientific Reports. 2025 Jul 23;15(1):26707. https://doi.org/10.1038/s41598-025-12319-6

5] Shetty AD, Shivamurthy B, Thimmappa BH, Parmar Y. Heat treatment and quenching effects on wear of electroless nickel–phosphorous plating. Cogent Engineering. 2021 Jan 1;8(1):1959009. https://doi.org/10.1080/23311916.2021.1959009

6] Zarebidaki A, Akbarpour M. Corrosion and wear behavior of electroless Ni-P-Cu coatings containing 8 and 18 wt% Cu. Surface and Coatings Technology. 2024 Sep 30;492:131228. https://doi.org/10.1016/j.surfcoat.2024.131228

7] Yazdani S, Vitry V. RSM models approach for optimization of the mechanical properties of electroless Ni-B-nanodiamond coating: An experimental and molecular dynamic simulation study. Surface and Coatings Technology. 2023 Jan 15;452:129133. https://doi.org/10.1016/j.surfcoat.2022.129133

8] Zhao C, Guo Y, Yang Y, Bai Y, Li B, Lu WF, Zeng K, Wang H. Effect of heat treatment and electroless Ni-P coating on mechanical property and corrosion behaviour of 316L stainless steel fabricated by laser powder bed fusion. Virtual and Physical Prototyping. 2024 Dec 31;19(1):e2312912. https://doi.org/10.1080/17452759.2024.2312912

9] Cheng K, Wu Z. Effect of heat treatment on the microstructure and mechanical properties of electroless nickel-phosphorus coatings. InJournal of Physics: Conference Series 2020 Apr 1 (Vol. 1520, No. 1, p. 012002). IOP Publishing. DOI 10.1088/1742-6596/1520/1/012002

10] Dang X, Cui K, Zhuang J, Zhong L, He Y, Li G, Du G, Yang Z, Pei S, Li S. A new environmentally friendly non-destructive activation process of electroless nickel plating on alumina ceramics. Materials Today Communications. 2023 Jun 1;35:105506. https://doi.org/10.1016/j.mtcomm.2023.105506

11] Sarkar S, Koley I, Baranwal RK, Mukherjee A, Lamichaney S, Majumdar G. Optimization of process parameters on the response of corrosion resistance of electroless Ni-Co-P coating using Box-Behnken Design (BBD). InJournal of Physics: Conference Series 2020 Jul 1 (Vol. 1593, No. 1, p. 012040). IOP Publishing. DOI 10.1088/1742-6596/1593/1/012040

12] Genova V, Paglia L, Pulci G, Pedrizzetti G, Pranzetti A, Romanelli M, Marra F. Medium and high phosphorous Ni-P coatings obtained via an Electroless approach: optimization of solution formulation and characterization of coatings. Coatings. 2023 Aug 24;13(9):1490. https://doi.org/10.3390/coatings13091490

13] Mousavi M, Rahimi E, Mol JM, Gonzalez-Garcia Y. The effect of phosphorous content on the microstructure and localised corrosion of electroless nickel-coated copper. Surface and Coatings Technology. 2024 Sep 30;492:131174. https://doi.org/10.1016/j.surfcoat.2024.131174

14] Qiao Y, Hou J, Lai M, Fang F. Control system and process optimization for electroless nickel plating. Nanotechnology and Precision Engineering. 2025 Jun 1;8(2). https://doi.org/10.1063/10.0034399

15] Kollabathini SS, Dora SP, Chintada S, Arava H. Influence of pH on the electroless Ni-P plating of SiC particles. Surface Engineering. 2025 Feb;41(2):217-26. https://doi.org/10.1177/02670844251320318

16] Omar R, A El-Sharief M. Optimization of electroless Ni-P coating bath and its impact in the Industrial Applications. JES. Journal of Engineering Sciences. 2021 Jan 1;49(1):42-52. DOI: 10.21608/jesaun.2021.51649.1022

17] Saravanan MS, Ananda V, Babu SK, Ramalingam G, Haiter Lenin A, Yimer JM, Sajin JB, Tharayil T. Properties Evaluation of Electroless Ni- Coated Low-Carbon Steels. Journal of Nanomaterials. 2022;2022(1):8497927. https://doi.org/10.1155/2022/8497927

18] Vijayanand M, Varahamoorthi R, Kumaradhas P. Artificial neural network modelling for average surface roughness in citrate stabilised electroless nickel boron coatings. Materials Today: Proceedings. 2022 Jan 1;49:2239-44. https://doi.org/10.1016/j.matpr.2021.09.335

19] Ghosh S, Bose B, Gaji S, Lakra AV, Debnath S, Ghosh S. Effect of Electroless Nickel Coating on Wear Rate of EN8 Steel. InIOP Conference Series: Materials Science and Engineering 2023 Sep 1 (Vol. 1291, No. 1, p. 012033). IOP Publishing. DOI 10.1088/1757-899X/1291/1/012033

20] Conti M, Paglia L, Genova V, Pedrizzetti G, Baiamonte L, Marra F. The effects of deposition parameters on the properties of NiCr coatings obtained by electroless plating. Chemical Engineering Transactions. 2023 Jun 30;100:427-32. https://doi.org/10.3303/CET23100072

21] Shi Q, Hu J, Cui H, Zhou W, Cai K, Wang W, Jia L, Wang S, Chen Y. Low-temperature electroless Ni-P plating on copper-based polyimide substrates for flexible printed circuits. Transactions of the IMF. 2025 Jul 4;103(4):219-24. https://doi.org/10.1080/00202967.2025.252425

22] Zou XF, Hu YJ, Long XB, Huang LY. Prediction and optimization of phosphorus content in electroless plating of Cr12MoV die steel based on PSO-BP model. Surfaces and Interfaces. 2020 Mar 1;18:100443. https://doi.org/10.1016/j.surfin.2020.100443

23] Li H, Huang H, Cai D, Xiao J, Yuan X, Zhu W, Lv L. ZrB2-Reinforced Electroless Ni-WP Composite Coating with Enhanced Corrosion and Wear Resistance in 3.5 wt.% NaCl Solution. International Journal of Electrochemical Science. 2026 Jan 13:101293. https://doi.org/10.1016/j.ijoes.2026.101293

24] Muraliraja R, Elansezhian R. Influence of nickel recovery efficiency on crystallinity and microhardness of electroless Ni–P coatings and optimisation using Taguchi technique. Transactions of the IMF. 2015 May 28;93(3):126-32. https://doi.org/10.1179/0020296715Z.000000000238

25] Mallick A, Mandal R, Mondal N, Sarkar S, Biswas N, Maji B, Majumdar G. Parametric optimization and minimization of corrosion rate of electroless Ni–P coating using Box-Behnken design and Artificial Neural Network. Results in Surfaces and Interfaces. 2024 May 1;15:100228. https://doi.org/10.1016/j.rsurfi.2024.100228

26] Wang X, Li C, Chen S, Du A, Ma R, Zhao X, Wang S, Fan Y. Study on properties of Al_2O_3-Ni-P nano-particle composite coating by ultrasonic electroless plating on AZ91D magnesium alloy. Matéria (Rio de Janeiro). 2024;29:e20240514. https://doi.org/10.1590/1517-7076-RMAT-2024-0514

27] THABASSOOM HA, Florence JF. OPTIMIZED ELECTROLESS NICKEL DEPOSITION ON MILD STEEL USING LAWSONE AS COMPLEXING AGENT. Surface Review and Letters. 2024 Nov 23:2550058. https://doi.org/10.1142/S0218625X25500581

28] Mei S, Xiao Z, Chen Z, Hu Z, Zou X, Xu Q, Zheng Q. Prediction and optimization of Aluminum content in Ni-P-Al2O3 composite coatings on GCr15 Steel Based on PSO-BP Neural Network. Surfaces and Interfaces. 2025 May 1;64:106319. https://doi.org/10.1016/j.surfin.2025.106319

29] Khdeir Y, Awad A. A comparison of heuristic algorithms for solving the traveling salesman problem. An-Najah University Journal for Research-A (Natural Sciences). 2024 Sep 1;39(1). DOI: 10.35552/anujr.a.39.1.230

30] Vijayanand M, Varahamoorthi R, Kumaradhas P, Sivamani S. Modelling and optimization of amphoteric surfactant concentration in electroless nickel boron coatings for maximum microhardness. Key Engineering Materials. 2023 Apr 28;943:19-30. https://doi.org/10.4028/p-0r8ii9

31] Meijuan T, Jian Z, Hai R. Electroless Plating Of Thick Amorphous Nickel-Phosphorus Coating on Sicp/Al Composite Surface By Double Zincate Pretreatment. Al Composite Surface By Double Zincate Pretreatment. 2022 Feb. http://dx.doi.org/10.2139/ssrn.4014082

32] Udayakumar M, Sivaganesan S, Sivamani S. One-factor-at-a-time approach for optimization of biodiesel synthesis from crude mahua oil. International Journal of Mechanical Engineering. 2022;7(1):1577-84. https://doi.org/10.1016/j.biortech.2005.03.014

33] Sarkar S, Baranwal RK, Biswas C, Majumdar G, Haider J. Optimization of process parameters for electroless Ni–Co–P coating deposition to maximize micro-hardness. Materials Research Express. 2019 Apr 1;6(4):046415. DOI 10.1088/2053-1591/aafc47

32] Abdel-Rahman MA, Hassan SE, El-Din MN, Azab MS, El-Belely EF, Alrefaey HM, Elsakhawy T. One-factor-at-a-time and response surface statistical designs for improved lactic acid production from beet molasses by Enterococcus hirae ds10. SN Applied Sciences. 2020 Apr;2(4):573. https://doi.org/10.1007/s42452-020-2351-x

34] Kraber S. Augmenting one-factor-at-a-time data to build a DOE. Journal of Plastic Film & Sheeting. 2023 Jan;39(1):15-8. https://doi.org/10.1177/8756087922114798

35] Siouri F, Abujaber F, Jaradat M, Mubarak A. Eco-Friendly and Efficient Extraction of Parabens from Cream Products Using Magnetic Cellulose Nanoparticles: A Promising Analytical Method. An-Najah University Journal for Research-A (Natural Sciences). 2025 Mar 23;40(1):85-90. https://doi.org/10.35552/anujr.a.40.1.2454

36] Salicio-Paz A, Ugarte I, Sort J, Pellicer E, García-Lecina E. Full optimization of an electroless nickel solution: boosting the performance of low-phosphorous coatings. Materials. 2021 Mar 18;14(6):1501. https://doi.org/10.3390/ma14061501

37] Choudhury BS, Sen RS, Oraon B, Majumdar G. Statistical study of nickel and phosphorus contents in electroless Ni–P coatings. Surface engineering. 2009 Jul;25(5):410-4. https://doi.org/10.1179/174329407X239081

38] Singh Tumrate C, Roy Chowdhury S, Mishra D. Development of regression model to predicting yield strength for different steel grades. InIOP Conference Series: Earth and Environmental Science 2021 Jun (Vol. 796, No. 1, p. 012033). IOP Publishing. doi:10.1088/1755-1315/796/1/012033

39] Radhi AB, Hammdi NI. Estimation of Lead and Cadmium in the Hair and Nails of Petrol Station Workers. An-Najah University Journal for Research-A (Natural Sciences). 2025 Jan 15;39(2):189-96. https://doi.org/10.35552/anujr.a.39.2.2372

40] Buenaño L, Ali E, Jafer A, Zaki SH, Hammady FJ, Khayoun Alsaadi SB, Karim MM, Ramadan MF, Omran AA, Alawadi A, Alsalamy A. Optimization by Box–Behnken design for environmental contaminants removal using magnetic nanocomposite. Scientific Reports. 2024 Mar 23;14(1):6950. https://doi.org/10.1038/s41598-024-57616-8

41] Chen HY, Chen C. Importance of using modern regression analysis for response surface models in science and technology. Applied Sciences. 2025 Jun 26;15(13):7206. https://doi.org/10.3390/app15137206

42] Vijayanand M, Varahamoorthi R, Kumaradhas P, Sivamani S. Modelling and optimisation of hardness in citrate stabilised electroless nickel boron (ENi-B) coatings using back propagation neural network–Box Behnken design and simulated annealing–genetic algorithm. Transactions of the IMF. 2021 Sep 3;99(5):253-64. https://doi.org/10.1080/00202967.2021.1898172